QUASI-ELASTIC PROTON KNOCKOUT FROM ^{16}O

KEES DE JAGER[a]
Thomas Jefferson National Accelerator Facility, Newport News, Va 23606, USA
E-mail: kees@jlab.org

In Hall A at Jefferson Lab, we have measured cross sections for quasielastic proton knockout in the ^{16}O$(e,e'p)$ reaction at ω = 0.44 GeV and Q^2 = 0.8 (GeV/c)^2 for missing momenta, p_m, up to 355 MeV/c. We have extracted the response functions R_{L+TT}, R_T, R_{LT}, and the left-right asymmetry A_{LT} for $E_m <$ 60 MeV. In contrast to some previous measurements at lower Q^2, our data for the valence states are well described by relativistic DWIA calculations. In the continuum, the cross sections and the response functions, for missing energies below 50 MeV and missing momenta below 150 MeV/c, are mostly accounted for by s-shell single-particle knockout calculations. R_L becomes small for missing energies higher than 50 MeV, while R_T remains substantial, suggesting the onset of non-single particle interactions. At $p_m \approx$ 280 MeV/c, R_L is consistent with zero and with theory, whereas the cross section, R_T and R_{LT} are much larger than the single-particle knockout calculations.

1 Introduction

The coincidence $(e,e'p)$ reaction in quasielastic kinematics ($\omega = Q^2/2m_p$ where Q and ω are the four-momentum and energy transfers and m_p the proton mass) has long been a crucial tool in the study of nuclear structure [1,2]. Measurements of the $(e,e'p)$ cross section have provided both a wealth of information on the wave functions of protons inside the nucleus and stringent tests of nuclear theories. Response function measurements have provided detailed information about the different reaction channels contributing to the cross section, such as single- and multi-nucleon knockout, meson-exchange currents, isobar excitations, relativistic effects and final-state interactions.

^{16}O$(e,e'p)$ $1p$-state proton knockout experiments have been performed at NIKHEF [3,4], Saclay [5,6], and Mainz [7] at low four-momentum transfer ($Q^2 < 0.4$ (GeV/c)^2) in various kinematics[b], resulting in spectroscopic factors by comparing data to Distorted Wave Impulse Approximation (DWIA) calculations. The published spectroscopic factors ranged between 0.5 and 0.7, except for

[a] for the Jefferson Lab Hall A collaboration

[b] The kinematic quantities are defined as follows: the scattered electron transfers momentum $\vec{q}$ and energy ω with $Q^2 = \vec{q}^2 - \omega^2$. The ejected proton has momentum $\vec{p}_p$ and kinetic energy T_p. The cross section is typically measured as a function of missing energy $E_m = \omega - T_p - T_{recoil}$ and missing momentum $p_m = |\vec{q} - \vec{p}_p|$. The angle between the ejected proton and virtual photon is θ_{pq} and the azimuthal angle is ϕ. Positive θ_{pq} corresponds to $\phi = 180^\circ$ and $\theta_p > \theta_q$. Negative θ_{pq} corresponds to $\phi = 0^\circ$.

those determined from the Blomqvist data [2].

Originally, the quasi-elastic cross section was attributed entirely to single-particle knockout from the valence states of the nucleus. However, ^{12}C$(e, e'p)$ coincidence data reported by Ulmer *et al.* [8] show a dramatic increase in the transverse-to-longitudinal ratio above the two-particle emission threshold. This enhancement indicates the presence of an extra, transverse, non-quasielastic reaction mechanism. The longitudinal response becomes consistent with zero above E_m= 50 MeV, indicating that single-particle knockout is very small above this point. A similar R_T/R_L enhancement has been observed at NIKHEF-K for ^{6}Li [9] and ^{12}C [10]. These findings indicate that a significant part of the cross section at large missing energies originates from two- and multi-body processes.

This paper reports the results [11] of the first experiment (E89-003 [12]) in Jefferson Lab Hall A [13], which measured the cross section[c], extracted A_{LT} and separated the response functions R_{L+TT}, R_T, and R_{LT} at quasielastic kinematics at $Q^2 = 0.8$ (GeV/c)^2 and $\omega = 0.44$ GeV for $p_m <$ 355 MeV/c.

2 The experiment

The continuous electron beam was scattered from a waterfall target [19], the scattered electrons were detected in the High Resolution Electron Spectrometer (HRSe) and the protons in the High Resolution Hadron Spectrometer (HRSh) [13]. The HRSe detector package consisted of two scintillator planes to generate the trigger, a gas Cherenkov detector for particle identification and a pair of two-plane Vertical Drift Chambers (VDCs) for trajectory determination. On HRSh only the VDCs and trigger scintillators were used for this experiment. The angle of the particle was determined [14,15,16] to 0.3 mrad and its absolute momentum [17] to $\frac{\delta p}{p} = 1.5 \times 10^{-3}$. We also surveyed [18] the central angles and offsets of each spectrometer at all positions to an accuracy of 0.02 mrad and 0.5 mm.

The waterfall target [19] consisted of three flat flowing water 'foils', each approximately 130 mg/cm^2 thick along the beam and at 30° to the incident beam. Using three foils improved the target energy-loss determination and

[c] In the first Born approximation the unpolarized $(e, e'p)$ cross section can be expressed as [2]

$$\frac{d^6\sigma}{d\Omega_e d\Omega_p d\omega dE_{p'}} = \frac{p' E_{p'}}{(2\pi)^3}\sigma_{Mott}(V_L R_L + V_T R_T + V_{LT} R_{LT}\cos\phi + V_{TT} R_{TT}\cos 2\phi), \quad (1)$$

where V_L, V_T, V_{LT} and V_{TT} are kinematic factors dependent upon the electron vertex and σ_{Mott} is the Mott cross section.

allowed the use of vertex cuts to reject accidentals. The hydrogen in the H_2O target greatly simplified the normalizations and calibrations. The luminosity was monitored by continuously measuring H(e, e) and $\vec{q}$ was determined by measuring H(e, ep) to an accuracy of 1.5×10^{-4}.

The cross section was measured at fixed $|\vec{q}| = 992$ MeV/c at three beam energies (corresponding to three virtual photon polarizations) to separate the response functions and understand our systematic uncertainties. We took data at the following kinematics: $E_{beam} = 2.442$ GeV, $\theta_{pq} = 0°, \pm 2.5°, \pm 8°, \pm 16°$, and $\pm 20°$; $E_{beam} = 0.843$ GeV, $\theta_{pq} = 0°, +8°$ and $+16°$; and $E_{beam} = 1.643$ GeV, $\theta_{pq} = 0°, \pm 8°$. The angles $0°, 2.5°, 8°, 16°$, and $20°$ correspond to central missing momenta of 53, 60, 148, 280, and 345 MeV/c, respectively. Note that at $\theta_{pq} = 0°$, we had to remove the data at p_m<45 MeV/c to eliminate contamination from H(e, ep).

For $\theta_{pq} = \pm 8°$, the values for R_{LT} and A_{LT} extracted at $E_{beam} = 2.4$ GeV agree with those extracted at $E_{beam} = 1.6$ GeV within one standard deviation. The overall systematic uncertainty in the extracted response functions is about 5%. This uncertainty is dominated by the uncertainty in the H(e, e) cross section to which the data were normalized[20].

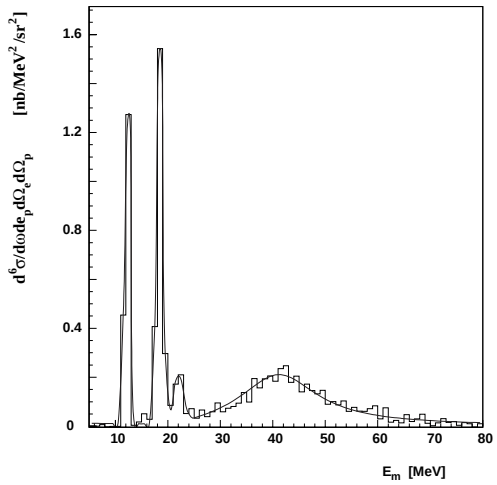

Figure 1: Measured ^{16}O$(e, e'p)$ missing energy spectrum for $E_{beam} = 2.4$ GeV at p_m= 60 MeV/c.

3 Valence states

The radiatively corrected ^{16}O$(e,e'p)$ cross section is shown in Fig. 1 as a function of E_m for $E_{beam} = 2.4$ GeV at $p_m \approx 60$ MeV/c. The two prominent peaks at $E_m = 12.1$ and 18.4 MeV correspond to protons knocked-out from the $1p_{1/2}$- and $1p_{3/2}$-states, respectively. The missing-energy resolution is 0.9 MeV FWHM, which does not allow separation of the $(2s_{1/2}, 1d_{5/2})$-doublet located at $E_m = 17.4$ MeV from the $1p_{3/2}$-state. The strength of this doublet has been estimated using the spectroscopic factors obtained by Leuschner *et al.* [3] It is predicted to be small for this kinematical region and has not been subtracted from the $1p_{3/2}$ cross section. The peak at 22 MeV corresponds to another $1p_{3/2}$-state. The broad peak centered at $E_m \approx 42$ MeV is due to proton knockout from the $1s_{1/2}$-state.

The first relativistic calculations for $(e,e'p)$ were performed by Picklesimer and Van Orden [21,22]. The present data were compared to more recent calculations by Udias *et al.* [23,24,25] and by Kelly [26]. Both calculations used the Coulomb gauge, the NLSH bound-state wave function [27], the energy-dependent EDAIO optical potential of Cooper *et al.* [28], the cc2 prescription of the off-shell e-p cross section [29], and include the effects of electron distortion. The NLSH wave function yields values of the binding and single-particle energies, as well as of the charge radius of ^{16}O, which are in good agreement with data. The primary difference between the two calculations is that Kelly solved a relativized Schrödinger equation and used the effective momentum approximation for the lower components of the Dirac spinors, while Udias *et al.* solved the Dirac equation directly in configuration space. The results for the $1p_{3/2}$-state from both calculations include an incoherent contribution from the positive-parity contaminants as parametrized by Leuschner *et al.* [3]

Figure 2 shows the measured p_m-distribution at $E_{beam} = 2.4$ GeV. Both calculations are in excellent agreement with the data. The spectroscopic factors are 0.73 and 0.72 for the $1p_{1/2}$-state and 0.71 and 0.67 for the $1p_{3/2}$-state for the calculations of Udias *et al.* and Kelly, respectively. Despite the large difference in Q^2, this data set is consistent with previous measurements, except for the spectroscopic factors determined from the Blomqvist data.

We extracted the left-right asymmetry ($A_{LT} = \frac{\sigma(\phi=0^\circ)-\sigma(\phi=180^\circ)}{\sigma(\phi=0^\circ)+\sigma(\phi=180^\circ)}$) from the measured cross sections (see Fig. 3). Note the large change in slope of A_{LT} at $p_m \approx 300$ MeV/c. This change in slope is reproduced, at least qualitatively, by both calculations, although only when the distortion of the lower components of the Dirac spinors is included. As is evident in Fig. 3 from the calculations of Udias *et al.*, distortion of the bound-state spinors is more important than that of the ejectile spinors, although both are needed.

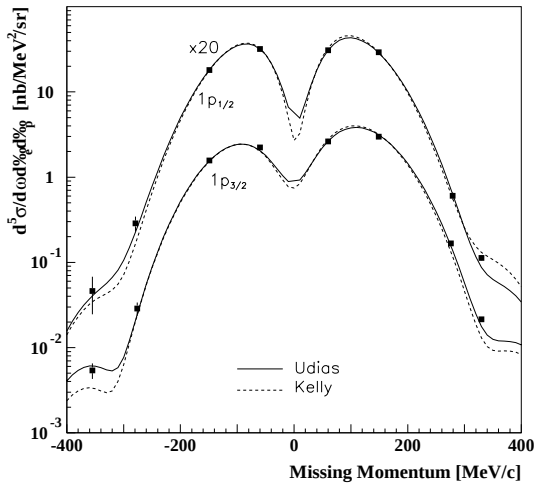

Figure 2: Measured cross sections and DWIA calculations at $E_{beam} = 2.4$ GeV. The solid line is the the Udias [25] and the dashed line the Kelly [26] calculation. The $1p_{1/2}$-state cross section and calculation have been multiplied by a factor of 20.

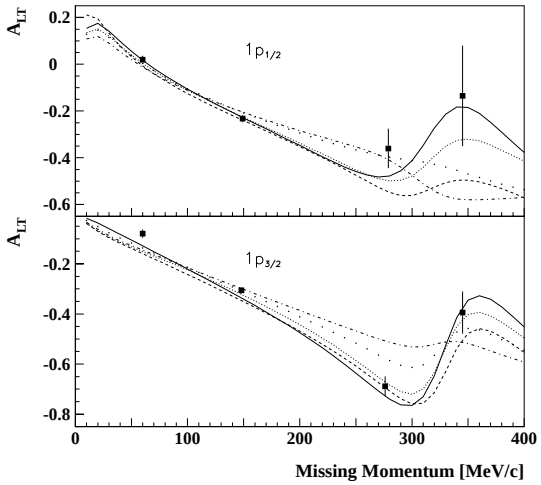

Figure 3: Measured left-right asymmetry A_{LT} and DWIA calculations at $E_{beam} = 2.4$ GeV. The dashed line is the Kelly [26] calculation. The rest of the curves are from Udias *et al.* [25,30]. The solid line is the fully relativistic calculation, the close-dotted line the calculation with only the bound-state spinor distortion included, the wide-dotted line with only the scattered-state spinor distortion included, and the dot-dashed line without any spinor distortion.

Kelly also sees an effect due to distortion of the bound-state spinors, but his calculations are not as accurate for $p_m >$ 275 MeV/c, due to approximations he makes.

We also extracted the response functions R_{L+TT}, R_{LT}, and R_T. Since the cross sections were measured in perpendicular kinematics, the longitudinal response function R_L could not be isolated. Instead, we extracted the combination $R_{L+TT} = R_L + \frac{V_{TT}}{V_L} R_{TT}$. Both Kelly and Udias predict that the contribution from R_{TT} is small ($< 10\%$) compared to R_L for these kinematics. Fig. 4 shows the response functions and calculations. Again, both calculations are in excellent agreement with the data. Moreover, neither calculation includes any two-body currents, suggesting that such currents are unimportant at this Q^2.

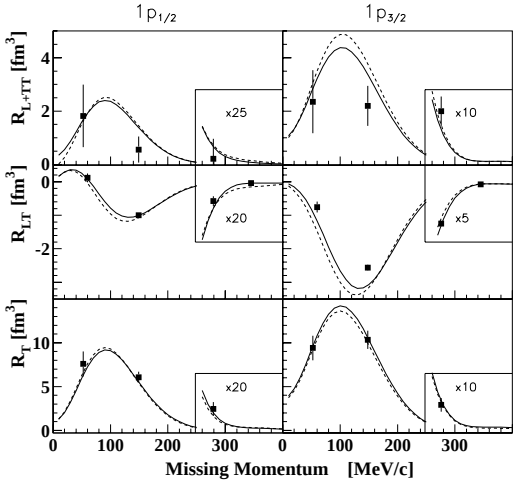

Figure 4: Measured R_{L+TT}, R_{LT} and R_T and the DWIA calculations. The solid line is the Udias *et al.* [25,30] calculation and the dashed line is the one from Kelly [26]. The data beyond 250 MeV/c missing momentum have been expanded for clarity.

4 Continuum knock-out

To check how much of the observed continuum strength can be explained by $1s_{1/2}$-knockout, we compared our results to $1s_{1/2}$ single-particle knockout calculations by Van Orden [21,22], Kelly [2] and Ryckebusch [31,32,33]. The Ryckebusch calculations (Impulse Approximation (IA) calculations and calculations that include two-body current contributions related to Meson Exchange Currents

(MECs) and Δ-creation) have been performed in a self-consistent Hartree-Fock (HF) frame work. The Kelly calculations are non-relativistic DWIA calculations, while the Van Orden calculations use the relativistic DWIA.

The calculated $1s_{1/2}$ response functions in E_m were distributed using a prescription given by Jeukenne and Mahaux [34,35], where the $1s_{1/2}$-profile is modeled using a Lorentzian with an energy-dependent width , (E).

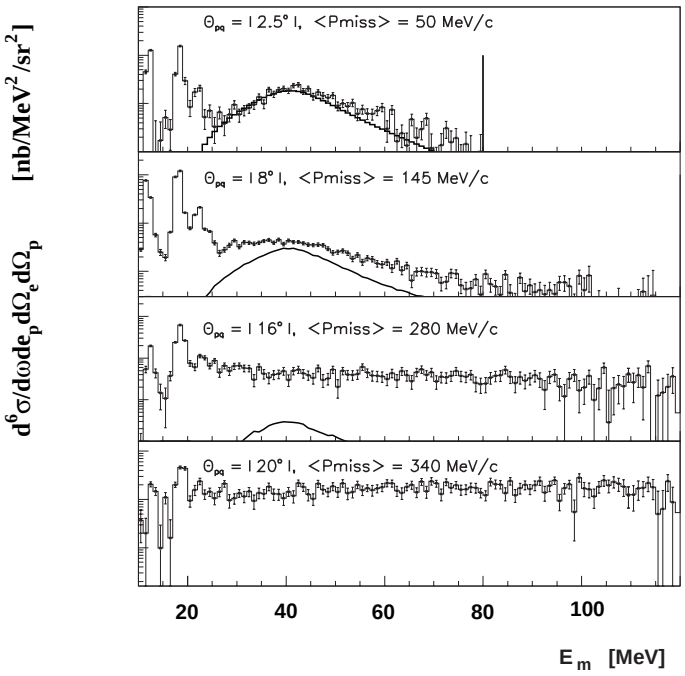

Figure 5: Cross section measured at different missing momenta as a function of missing energy. The solid lines show the $1s_{1/2}$ single-particle strength calculated by Van Orden folded in with the energy-dependent Lorentzian parameterization by Mahaux. The s-shell spectroscopic factor used with the calculation was determined by fitting to the $\theta_{pq} = 2.5°$ data (top plot).

Figure 5 shows the cross section measured over the whole range of missing momenta covered by this experiment. The cross-section data are compared to $1s_{1/2}$ single-particle knockout calculations by Van Orden [21,22] folded in with the energy-dependent Lorentzian parameterization by Mahaux. At $<p_m>= 50$ MeV, the Lorentzian shape exactly explains the measured cross section. The spectroscopic factor used with all Van Orden calculations presented here was

determined by fitting to these data. For the $1s_{1/2}$-shell the spectroscopic factor thus determined was 0.88, which is significantly higher than previously reported spectroscopic factors for the $1s_{1/2}$-shell [36].

As p_m increases, the single-particle knock-out calculation accounts for only a fraction of the measured strength. Furthermore, for the two settings with p_m above the Fermi momentum, the measured cross section profiles do not exhibit any resemblance to the expected $1s_{1/2}$ Lorentzian shape. This clearly indicates that the cross section measured at high p_m and high E_m is mostly of non-single particle origin. For $45 < p_m < 75$ MeV/c, R_L and R_T are close to DWIA and HF models of s-shell knockout. The difference between the transverse and longitudinal spectral functions, which is expected to be zero for a free nucleon, is non-zero for $E_m > 40$ MeV. This is in qualitative agreement with previous observations [8,9,10]. At $p_m \sim 150$ MeV/c R_L and R_T are mostly accounted for by the DWIA and HF models of s-shell knockout for $E_m < 50$ MeV. For $E_m > 50$ MeV , R_T remains strong while R_L appears to go to zero.

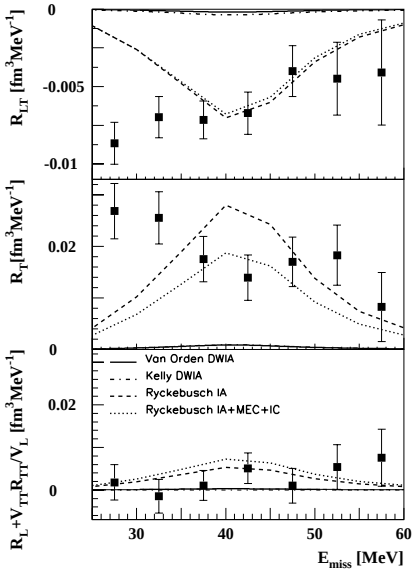

Figure 6: Separated response functions for the $|\theta_{pq}| = 16°$ setting ($<p_m> \approx 280.0$ MeV/c). Plots show (from top to bottom) R_{LT}, R_T, and $R_L + \frac{V_{TT}}{V_L} R_{TT}$.

Figure 6 presents the separated response functions for the $|\theta_{pq}| = 16°$ perpendicular kinematic setting, $p_m \approx 280$ MeV/c. $R_L + V_{TT} R_{TT}/V_L$ is close

to zero, as predicted by all three calculations. R_T and R_{LT} appear to slowly decrease over 25 $<E_m<$ 60 MeV, but the data are much larger than the DWIA calculations and close to the HF calculations. Neither R_T nor R_{LT} show a peak at $E_m \approx$ 40 MeV corresponding to single-particle knockout from the s-shell.

5 Summary

In summary, we have studied, in a previously inaccessible region of momentum transfer, ^{16}O$(e,e'p)$ proton knockout for missing momentum less than 355 MeV/c. The measurements for the valence $1p$-state yielded the cross section, the left-right asymmetry A_{LT}, and the response functions R_{L+TT}, R_{LT}, and R_T. Structure in A_{LT} is observed at higher p_m which is due to a dynamic enhancement of the lower components of the Dirac spinors. Our cross sections, asymmetries and response functions are in excellent agreement with the recent relativistic DWIA calculations without the inclusion of two-body currents. For knock-out from the continuum at low p_m- and low E_m-values the DWIA single-particle calculations account for most of the observed continuum strength, but as p_m increases, for only a fraction of the measured strength, while the measured cross section profiles do not exhibit any resemblance to the expected $1s_{1/2}$ Lorentzian shape. This suggests that the cross section measured at high p_m and high E_m is mostly of non-single particle origin.

Acknowledgments

We acknowledge the outstanding support of the Hall A technical staff and of the staff of the Accelerator Division of Jefferson Laboratory that made this experiment successful. We thank T.W. Donnelly, J.J. Kelly, J.M. Udias, J. Ryckebusch and J.W. Van Orden for providing their theoretical calculations and for valuable discussions. This work was supported in part by the U.S. Department of Energy, the National Science Foundation, the Italian Institute for Nuclear Research, the French Atomic Energy Commission and National Center of Scientific Research and the Natural Sciences and Engineering Research Council of Canada.

References

1. S. Frullani and J. Mougey, *Adv. Nucl. Phys.* **14**, 1 (1984).
2. J.J. Kelly, *Adv. Nucl. Phys.* **23**, 75 (1996).
3. M. Leuschner *et al.*, *Phys. Rev.* C **49**, 955 (1994).
4. C.M. Spaltro *et al.*, *Phys. Rev.* C **48**, 2385 (1993).
5. M. Bernheim *et al.*, *Nucl. Phys.* A **375**, 381 (1982).

6. L. Chinitz *et al.*, *Phys. Rev. Lett.* **67**, 568 (1991).
7. K.I. Blomqvist *et al.*, *Phys. Lett.* B **344**, 85 (1995).
8. P.E. Ulmer *et al.*, *Phys. Rev. Lett.* **59**, 2259 (1987).
9. J.B.J.M. Lanen *et al.*, *Phys. Rev. Lett.* **64**, 2250 (1990).
10. G. van der Steenhoven *et al.*, *Nucl. Phys.* A **480**, 547 (1988).
11. www.jlab.org/ fissum/e89003.html.
12. A. Saha, W. Bertozzi, R.W. Lourie, and L.B. Weinstein, Jefferson Lab Proposal E89-003; K.G. Fissum, MIT-LNS Internal Report #02, 1997.
13. www.jlab.org/Hall-A/equipment/HRS.html.
14. N. Liyanage *et al.*, MIT-LNS Internal Report #05, 1998.
15. J. Gao, *Ph.D. thesis*, MIT, 1999 (unpublished).
16. N. Liyanage, *Ph.D. thesis*, MIT, 1999 (unpublished).
17. J. Gao *et al.*, MIT-LNS Internal Report #04, 1998.
18. M. Liang, *Survey Summary Report*, Jefferson Lab Technical Note JLAB-TN-99029.
19. F. Garibaldi *et al.*, *Nucl. Instrum. Methods* A **314**, 1 (1992).
20. G.G. Simon *et al.*, *Nucl. Phys.* A **333**, 381 (1980); L.E. Price *et al.*, *Phys. Rev.* D **4**, 45 (1971).
21. A. Picklesimer, J.W. Van Orden, and S.J. Wallace, *Phys. Rev.* C **32**, 1312 (1985).
22. A. Picklesimer and J.W. Van Orden, *Phys. Rev.* C **40**, 290 (1989).
23. J.M. Udias *et al.*, *Phys. Rev.* C **48**, 2731 (1993).
24. J.M. Udias *et al.*, *Phys. Rev.* C **51**, 3246 (1995).
25. J.M. Udias *et al.*, nucl-th/9905030.
26. J.J. Kelly, nucl-th/9905024.
27. M.M. Sharma, M.A. Nagarajan and P. Ring, *Phys. Lett.* B **312**, 377 (1993).
28. E.D. Cooper, S. Hama, B.C. Clark, and R.L. Mercer, *Phys. Rev.* C **40**, 297 (1993).
29. T. De Forest, *Nucl. Phys.* A **392**, 232 (1983).
30. J.M. Udias, private communication.
31. J. Ryckebusch *et al.*, *Nucl. Phys.* A **476**, 237 (1988).
32. J. Ryckebusch *et al.*, *Nucl. Phys.* A **503**, 694 (1989).
33. V. Van der Sluys, K. Heyde, J. Ryckebusch, M. Waroquier, *Phys. Rev.* C **55**, 1982 (1997).
34. J. Ryckebusch *et al.*, *Nucl. Phys.* A **624**, 581 (1997).
35. J.P. Jeukenne and C. Mahaux, *Nucl. Phys.* A **394**, 445 (1983).
36. W. Bertozzi, *Nucl. Phys.* A **527**, 347c (1991).